Slow-light: Fascinating physics or potential applications?

Slow-light through nonlinear wave-mixing in liquid crystal light-valves

Umberto Bortolozzo [a], Stefania Residori [a,*], Jean-Pierre Huignard [b]

[a] *Institut non linéaire de Nice, université de Nice Sophia-Antipolis, CNRS, 1361 route des Lucioles, 06560 Valbonne, France*
[b] *Thales Research & Technology, RD 128, 91767 Palaiseau cedex, France*

Available online 30 December 2009

Abstract

Slow-light is obtained through nonlinear wave-mixing in a liquid crystal light-valve. A deceleration of light pulses down to group velocities as small as 0.2 mm/s is achieved when two-wave-mixing is performed with a continuous pump and a time modulated signal. A model accounts for the observations in the general framework of nonlinear wave-mixing in thin media. The large group delay provided by the light-valve is exploited to enhance the spectral sensitivity of an interferometer, whereas the narrow frequency bandwidth of the two-wave-mixing gain is used to realize an adaptive holographic system that allows achieving subpicometer detection. ***To cite this article: U. Bortolozzo et al., C. R. Physique 10 (2009).***
© 2009 Académie des sciences. Published by Elsevier Masson SAS. All rights reserved.

Résumé

Lumiére lente par mélange d'ondes non linéaire dans les valves optiques à cristaux liquides. Dans une valve optique à cristaux liquides, des processus non linéaires de mélange d'ondes permettent d'obtenir la lumière lente. Les impulsions lumineuses sont ralenties jusqu'à des vitesses de groupe aussi petites que 0.2 mm/s. Un modèle décrit les observations dans le cadre général des processus d'interaction dans les milieux minces. Le grand retard de groupe fourni par la valve optique est exploité pour augmenter la sensibilité d'un interféromètre, alors que l'étroite bande de fréquence associée au gain du mélange à deux ondes est utilisée pour réaliser un système d'holographie adaptative qui permet la détection d'une fraction de picomètre. ***Pour citer cet article : U. Bortolozzo et al., C. R. Physique 10 (2009).***
© 2009 Académie des sciences. Published by Elsevier Masson SAS. All rights reserved.

Keywords: Slow-light; Liquid crystals; Light-valves; Nonlinear wave-mixing; Adaptive holography

Mots-clés : Lumière lente ; Cristaux liquides ; Valves optiques ; Mélange d'ondes ; Holographie adaptative

1. Introduction

Slow- and fast-light effects are attracting a lot of attention because of their interest both from the fundamental point of view and for applications [1]. Indeed, the ability to control the velocity of light pulses is crucial in several domains, for example for the realization of all-optical communication networks [2], in high sensitivity interferometers
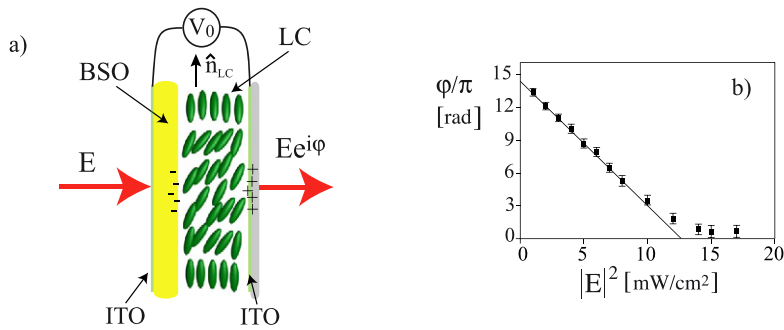

Fig. 1. (Color online.) (a) Schematic representation of the liquid crystal light-valve (LCLV): the liquid crystal (LC) layer is inserted in between a photoconductor (BSO) and a glass wall; transparent ITO electrodes allow the application of an external voltage V_0. (b) Typical response of the LCLV: the phase shift φ of the output beam is plotted as a function of the input intensity $|E|^2$.

[3], in precision metrology and optical sensing [4]. Moreover, fast-light has been proposed as a method to enhance the sensitivity of gravitational wave detectors, which has been tested by employing atomic vapors [5] or double pumped two-wave-mixing in photorefractive crystals [6]. Early achievements of slow-light were obtained by exploiting electromagnetically induced transparency in ultracold atoms [7–9]. Then, slow-light was realized at room temperature by employing a mechanism called coherent population oscillation, which creates spectral holes in the absorption spectrum of a solid crystal [10]. Nowadays, different methods to realize slow- and fast-light effects are currently employed, such as, for example, active control in photonic crystal waveguides [11,12] or in semiconductor structures [13,14].

Among the different mechanisms, the processes of nonlinear wave-mixing offer the advantage of large and tunable dispersion properties, which can be used to obtain controllable group velocities in small-sized, room temperature experiments. Nonlinear wave-mixing processes have been extensively studied in the past, leading to a large number of attractive effects, from which we can cite, for instance, real-time holography and dynamic gratings [15], sensitivity enhanced interferometry [16], optical amplification [17] and optical phase conjugation [18]. All these processes rely on the coherent coupling between two or more optical beams, inducing a nonlinear excitation in the medium to which is associated a large, usually tunable, dispersion. These properties have been exploited for controlling the group velocity of light pulses, for example, in photorefractive crystals close to the Bragg resonance of the two-wave-mixing process [19–21] and in optical fibers through stimulated Brillouin scattering [22,23].

Recently, we have shown that by using a liquid crystal light-valve (LCLV) and by performing two-wave-mixing experiments in the Raman–Nath regime of diffraction, fast- and slow-light effects can be obtained with group velocities as slow as a few tenths of mm/s [24]. In the LCLV the wave-mixing process is characterized by the presence of multiple-order output beams, each experiencing a different group delay. On each output order, the group delay can be controlled by changing the frequency detuning between the pump and probe as well as by varying the external voltage applied to the light-valve. Another interesting property of the LCLV is related to its large transverse section that allows delaying whole images, a slow-light feature that was firstly demonstrated in atomic vapor experiments [25] and that could be used for image detection and storage [26] or wavefront sensing.

2. The liquid crystal light-valve

The liquid crystal light-valve is schematically depicted in Fig. 1a. It is made by associating a liquid crystal (LC) layer with a photorefractive $Bi_{12}SiO_{20}$ (BSO) crystal, cut in the form of a thin plate (1 mm thickness, 20×30 mm^2 lateral size) [27,28]. The BSO acts as one of the confining wall whereas the other wall is a glass window. The thickness of the LC layer is $d = 14$ μm. While liquid crystals are used for their large birefringence, the BSO is used for its large photoconductivity and transparency in the visible range [29]. Transparent electrodes (*Indium Tin Oxide*, ITO, layers) deposited over the BSO and the glass wall, allow the application of an external voltage V_0 across the LC layer. The voltage applied is a.c., with a r.m.s. value from 2 to 20 V and a frequency from 50 Hz to 20 kHz. The liquid crystals are nematic E48. The nematic phase is characterized by a long range orientational order for which all the molecules are aligned, in average, along a preferential direction, so called the nematic director $\hat{n}_{LC}$ [30]. Since the molecules have a different polarizability along their long and short axis, when an electric field, or a voltage V_0, is applied across

the nematic layer, an induced dipole moment arises and all the molecules reorient towards the direction of the applied field.

Because of the LC birefringence, the nematic layer as a whole behaves like a strongly birefringent material, characterized by a different refractive index for a beam polarized along the long or short molecular axis, so called, respectively, the extraordinary n_e and the ordinary n_o index. Typical values for nematics are $n_e = 1.7$ and $n_o = 1.5$, which gives a large birefringence $\Delta n = n_e - n_o = 0.2$. Therefore, when the LC molecules reorient under the action of an applied field, their collective motion implies a change of the principal axis of the nematic layer and, hence, an incoming light field experiences a large refractive index change. When a light beams impinges onto the LCLV, photo-generation of charges occurs at the BSO surface because of its photoconductive properties. Hence, the local voltage across the LC layer increases inducing a further molecular reorientation and, thus, an additional refractive index change. As a result, at the exit of the LCLV the light beam acquires a phase shift φ that is a function of the applied voltage and of the beam intensity.

A typical response of the LCLV is shown in Fig. 1b, where the phase shift φ acquired by the light beam when passing through the valve is plotted against the input beam intensity $I = |E|^2$. The response is linear up to intensities of the order of 10 mW/cm^2. Then, it saturates to a value that corresponds to the maximum LC birefringence, $\Delta n = 0.2$, for which all the LC molecules are aligned along the direction of the applied field. In between, that is, from the initial planar alignment and the final orthogonal alignment, the reorientation angle of the LC molecules varies from 0 to $\pi/2$ producing a phase shift φ of several π. In the linear region of its response, the LCLV behaves as a Kerr-like nonlinear medium, providing a refractive index change proportional to the input intensity $n = n_0 + n_2 I$, where n_0 is the value fixed by the applied voltage and n_2 is the nonlinear coefficient $\partial n/\partial I$. Thanks to the large LC birefringence, the nonlinear coefficient, which is the slope of the linear part of the response curve, is as large as $n_2 = -6$ cm^2/W, the minus sign accounting for the defocussing character of the nonlinearity (the refractive index changes from n_e to n_o, with $n_e > n_o$).

The response time of the LCLV is dictated by the time τ_{LC} required by the collective motion of the LC molecules to establish over the whole thickness d of the nematic layer. This is given by

$$\tau_{\mathrm{LC}} = \frac{\gamma}{K} d^2 \tag{1}$$

where γ is the LC rotational viscosity and K the splay elastic constant [30]. For $d = 14$ μm and typical values of the LC constants, τ_{LC} is of the order of 100 ms. The spatial resolution, which is the minimal size of an independently addressed area, is given by the electric coherence length of the LC,

$$l_{\mathrm{LC}} = \sqrt{\frac{\Delta \varepsilon}{K}} \frac{d}{V_0} \tag{2}$$

where $\Delta \varepsilon$ is the dielectric anisotropy of the LC, and, for the usual values of V_0, it is typically of the order of 10 μm.

3. Nonlinear wave-mixing in thin media: Theoretical background

Nonlinear wave-mixing in thin media implies beam coupling in the Raman–Nath regime of optical diffraction. Different with the Bragg regime, for which the phase matching condition is satisfied in only one direction [19–21], the Raman–Nath diffraction produces several output order beams [31]. Here, we will focus on the two-wave-mixing interaction that is used for obtaining slow- and fast-light effects in the LCLV. The interaction scheme and the essential setup for performing two-wave-mixing experiments in the LCLV are sketched in Fig. 2. A pump beam E_p is sent onto the LCLV together with a weaker signal beam E_s. The total electric field at the input of the LCLV can be written as

$$E_{\mathrm{in}}(\vec{r}, t) = E_s e^{i[\vec{k}_s \cdot \vec{r} - \omega_s t]} + E_p e^{i[\vec{k}_p \cdot \vec{r} - \omega_p t]} + \text{c.c.} \tag{3}$$

where E_p and E_s are the amplitudes of the pump, respectively, the signal wave, $\vec{k}_p$ and $\vec{k}_s$ their respective propagation vectors and ω_p, ω_s their frequencies. The two beams produce an intensity fringe pattern

$$\left| E_{\mathrm{in}}(\vec{r}, t) \right|^2 = I_T \left[1 + 2 \frac{E_p E_s}{I_T} \cos(\vec{K}_g \cdot \vec{r} - \Delta \omega \cdot t) \right] \tag{4}$$
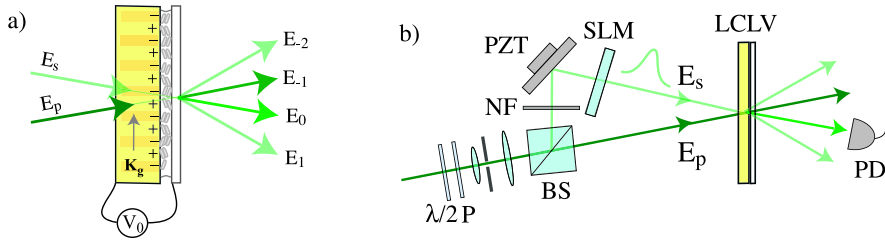
Fig. 2. (Color online.) (a) Schematic representation the two-wave mixing in the LCLV. (b) Experimental setup; $\lambda/2$: half-wave plate, P: polarizer, NF: neutral density filter, PZT: piezoelectrically driven mirror, SLM: spatial light-modulator, PD: photodiode.

where $I_T \equiv |E_s|^2 + |E_p|^2 = I_s + I_p$ is the total input intensity, $\vec{K}_g = \vec{k}_p - \vec{k}_s$ is the grating wave vector and $\Delta\omega = \omega_p - \omega_s$ the frequency detuning between the pump and signal. The ratio between the pump and signal intensity $\beta \equiv I_p/I_s$, is usually much larger than one.

The fringe pattern induces, on its turn, a photo-induced space charge distribution, hence a molecular reorientation pattern in the LC layer, which creates a refractive index grating with the same wave vector $\vec{K}_g$. The spatial period of the grating $\Lambda \equiv 2\pi/K_g$, is usually in between 50 and 300 µm. Because the thickness of the LC layer is much less than Λ, the LC grating acts as a thin hologram, thus, beam diffraction occurs in the Raman–Nath regime. Several diffracted beams, distinguished by the numbers $0, \pm 1, \pm 2, \ldots, \pm m$, are observed at the output of the LCLV. In Fig. 2 the output orders are identified as E_m. Due to self-diffraction, photons from the pump are transferred into the different output orders. The $m = 0, +1, \pm 2, \ldots$ orders are amplified, that is, they receive from the pump more photons than they are losing due to the scattering on the other orders. The $m = -1$ order is the pump beam that, even though depleted, remains of much higher intensity than the other beams [32].

To derive the full expression for the output field, we have to consider the evolution of the amplitude $n(\vec{r}, t)$ of the refractive index grating. This is governed by a relaxation equation following the molecular orientation dynamics of the LC [30]

$$\tau_{\mathrm{LC}} \frac{\partial n}{\partial t} = -\left(1 - l_{\mathrm{LC}}^2 \nabla^2\right)n + n_0 + n_2 |E_{\mathrm{in}}|^2 \tag{5}$$

where $l_{\mathrm{LC}} = 10$ µm is the transverse diffusion length, $n_0 = 1.6$ is the constant value of the refractive index given by the average LC orientation under the application of the voltage V_0, and $n_2 \simeq -6$ cm^2/W is the equivalent Kerr-like coefficient of the LCLV. By coupling the above Eq. (5) with the wave propagation equation for the input electric field, it can easily been shown that the m output order field can be written as [33]

$$\tilde{E}_m = E_m e^{i(\vec{k}_m \cdot \vec{r} - \omega_m t)} + \mathrm{c.c.} \tag{6}$$

where $\omega_m = \omega_s - m\Delta\omega$ is the frequency, $\vec{k}_m = \vec{k}_s - m\vec{K}_g$ the wave vector and the amplitude is given by

$$E_m = \left[E_s J_m(\rho) + i E_p J_{m+1}(\rho) e^{-i\Psi}\right] \cdot e^{i[k(n_0 + k n_2 I_T)z + m(\frac{\pi}{2} - \Psi)]} \tag{7}$$

where J_m is the Bessel function of the first kind and of order m,

$$\rho = \frac{2k n_2 E_p E_s}{\sqrt{(1 + l_{\mathrm{LC}}^2 K_g^2)^2 + (\Delta\omega \cdot \tau_{\mathrm{LC}})^2}} d \tag{8}$$

and

$$\tan\Psi = \frac{\Delta\omega \cdot \tau_{\mathrm{LC}}}{1 + l_{\mathrm{LC}}^2 K_g^2} \tag{9}$$

From the above expression (7), we see that each order m receive two contributions, one is the scattering of the signal and the other is the scattering of the pump onto the refractive index grating.

It is now useful to write each output order field in the form

$$\tilde{E}_m = \sqrt{G_m} E_s e^{i\Phi_m} e^{i(\vec{k}_m \cdot \vec{r} - \omega_m t)} + \mathrm{c.c.} \tag{10}$$
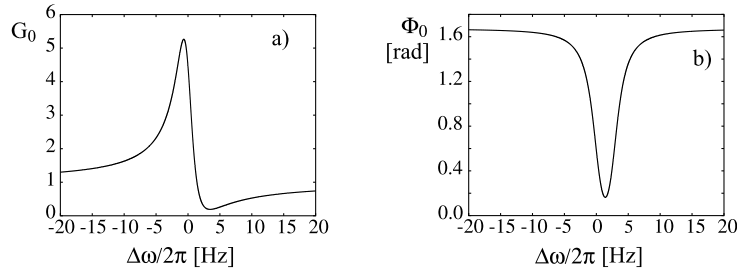
Fig. 3. (a) Gain G_0 and (b) phase shift Φ_0 for the $m = 0$ output order beam as a function of the frequency detuning $\Delta\omega$ between the pump and signal, $\beta = 30$.

where we define $G_m = |E_m|^2/|E_s|^2$ as the gain amplification factor and Φ_m is the associated nonlinear phase shift. Both G_m and Φ_m can be calculated from Eq. (7).

To understand the basic mechanism for slow- and fast-light, let us first consider only the $m = 0$ order, which coincides with the original propagation direction of the signal,

$$\tilde{E}_0 = \sqrt{G_0} E_s e^{i\Phi_0} e^{i(\vec{k}_s \cdot \vec{r} - \omega_s t)} + \text{c.c.} \tag{11}$$

The envelope amplitude can also be written as

$$E_0 = \left[E_s J_0(\rho) + i E_p J_1(\rho) e^{-i\Psi} \right] e^{i[k(n_0 + kn_2 I_T)z]} \tag{12}$$

from which we see that the two contributions, namely the scattering of the signal and the scattering of the pump, sum up with their relative phases. The final effect is to produce a gain with a narrow frequency bandwidth. In Fig. 3 the gain and phase curves, G_0 and Φ_0, are plotted as a function of the frequency detuning $\Delta\omega$ for parameter values close to the typical experimental conditions, $\tau_{LC} = 120$ ms, $l_{LC} = 15$ μm, $\Lambda = 150$ μm, $n_0 = 1.63$, $n_2 = -6$ cm^2/W and $\beta = 30$. The maximum gain and phase shift are obtained for $\Delta\omega \sim 0$. In correspondence, a temporally modulated signal will experience a large dispersion, as given by the large slope of the Φ_0 curve on both sides around $\Delta\omega = 0$. By changing the frequency detuning, and thus exploiting either the positive or negative slope of the dispersion curve, both slow- and fast-light effects can be achieved, as we will see in the following section.

4. Two-wave-mixing experiments: Slow- and fast-light

Slow- and fast-light effects in the LCLV are obtained by using the two-wave-mixing setup represented in Fig. 2b, where the beam coupling is realized with a continuous pump and a time modulated signal. The two beams originate from a cw solid state laser, $\lambda = 532$ nm. They are enlarged and collimated, the beam diameter on the LCLV is 18 mm. The light polarization is linear and parallel to the LC nematic director $\hat{n}_{LC}$. The intensity of the pump beam is fixed to $I_p = 1.8$ mW/cm^2 whereas the signal beam is time-modulated, by using a spatial-light modulator (SLM), to obtain a Gaussian wave packet with a width in between 100 and 200 ms, larger than the LC response time. The center frequency of the signal pulse can be changed by a few Hz with a piezoelectrically driven mirror (PZT) and its peak intensity is kept much less than the pump intensity, β being usually fixed to 30. The voltage applied to the LCLV is 20 V r.m.s. at a frequency of 1 kHz. On each diffracted order, a photodiode records the temporal evolution of the output beam, which is compared to the temporal evolution of the input signal.

Different group delays can be obtained depending on the output order considered and on the frequency detuning $\Delta\omega$ between the pump and signal. Two representative data taken, respectively, on the $m = -2$ and $m = 0$ order are shown in Fig. 4, showing an anticipated, fast-light, and a delayed, slow-light, pulse. Fast-light occurs for $\Delta\omega/2\pi = 3$ Hz, which is close to the minimum of the gain, therefore the pulse is attenuated, whereas slow-light is obtained for $\Delta\omega = 0$, which is close to the maximum of the gain. Therefore, the slow-light pulse is not only delayed but also amplified. By fitting each pulse with a Gaussian, we have evaluated the time anticipation as $\Delta t_0 = -65$ ms for the fast pulse and the time retardation as $\Delta t_{-2} = 110$ ms for the slow pulse. The effective group velocity of each pulse can be determined as $v_m = d/\Delta t_m$, where d is the thickness of the traversed LC layer and Δt_m the group delay of the order m. We obtain $v_0 = -0.21$ mm/s for the fast pulse and $v_{-2} = 0.13$ mm/s for the slow pulse.
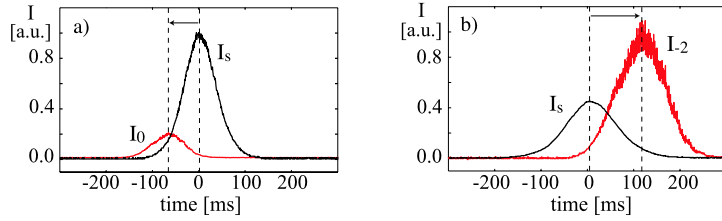
Fig. 4. (Color online.) Experimental time dependencies of the output pulse (red lines) taken on the (a) $m = 0$ and (b) $m = -2$ diffraction order of the input pulse (black line) showing, respectively, an anticipated (fast-light) and a delayed (slow-light) pulse.
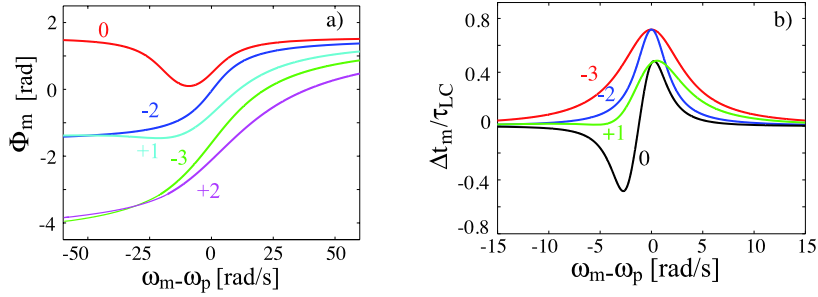

Fig. 5. (Color online.) (a) Dispersion curves Φ_m and (b) corresponding group delay Δt_m as a function of the frequency $(\omega_m - \omega_p)$ of the m output order; $\beta = 30$.

4.1. Tuning the group delay

As we have seen above, two-wave-mixing in the LCLV produces multiple output order beams. Associated to each order there is a gain and a dispersion curve that can be calculated from the model above, Eq. (7). A light pulse, that is, a wave packet, is composed by many optical frequencies, each corresponding to a distinct Fourier component propagating with its own phase velocity. For the pulse to propagate without distortion, all the frequency components have to keep in phase, which, mathematically, can be expressed by requiring that the wave packet as a whole propagate with the group velocity [1]

$$v_g = \frac{d\omega}{dk} = \frac{c}{n + \omega\, dn/d\omega} \tag{13}$$

where $dn/d\omega$ is the dispersion of the traversed medium. Formally, we can also express Eq. (13) as $v_g = c/n_g$, where n_g is the group index $n_g \equiv n + \omega\, dn/d\omega$. Controlling the group velocity can thus be realized by controlling the dispersion properties of the medium. For $dn/d\omega$ large and positive, the group index becomes very large and, correspondingly, the group velocity very small, $0 < v_g \ll c$, so that slow-light is achieved. On the other side, when $dn/d\omega$ is negative and large, the group velocity becomes negative, $v_g < 0$ and fast-light is achieved. Correspondingly, the group delay $\tau_g = d/v_g$, where d is thickness of the traversed medium, is large and becomes positive or, respectively, negative.

For the two-wave-mixing in the LCLV, the group delay Δt_m can be calculated for each output order m, and it is given by the slope of the dispersion curves

$$\Delta t_m = \frac{\partial \Phi_m}{\partial \omega_m} \tag{14}$$

In Fig. 5a the dispersion curves Φ_m, calculated for the same parameter values given above, are plotted for different orders m against $\omega_m - \omega_p$. Note that $\omega_m = \omega_s - m\Delta\omega$, thus the plot of Φ_m against $\Delta\omega$ would change sign for odd m. We have chosen to display Φ_m as a function of $\omega_m - \omega_p$, so that the slopes of the dispersion curves in the graph give directly the correct sign for the group delay. In Fig. 5b, the group delay Δt_m is plotted against $\omega_m - \omega_p$. From these curves, the group velocity of each output pulse can be calculated as $v_m \equiv d/\Delta t_m$ with d the thickness of the LC layer. We can note that fast-light is obtained on the $m = 0$ order. Moreover, for every m the slope of the Φ_m curves
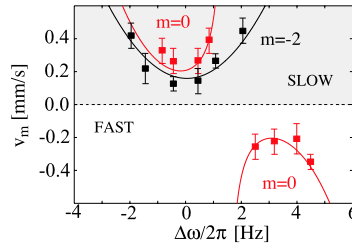
Fig. 6. (Color online.) Group velocity v_g vs $\Delta\omega/2\pi$ for $m = 0$ (red) and $m = -2$ (black); lines are theoretical, squares are experimental points.
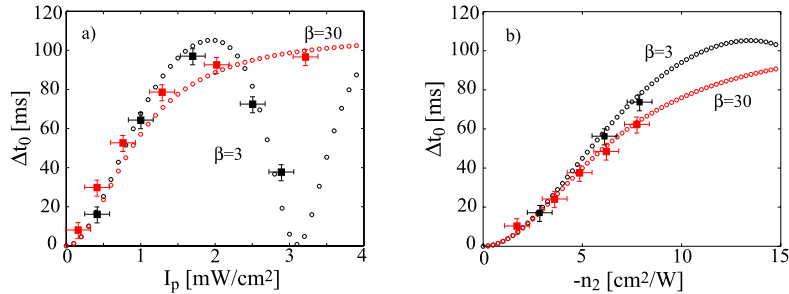

Fig. 7. (Color online.) Group delay Δt_0 as a function of (a) the pump intensity I_p and (b) the nonlinear coefficient n_2; black dots: $\beta = 3$, red dots: $\beta = 30$. Black and red squares are experimental points measured for $\beta = 3$ and 30, respectively.

is maximum for $\omega_m = \omega_p$, hence the maximum group delay is obtained when the pump and signal have the same frequency. The theoretical limit for the maximum group delay can be calculated analytically and it is given by

$$\Delta t_m^{(max)} = \frac{m}{m+1}\tau_{LC} + \frac{1}{m+1}\left[\frac{\beta(\frac{J_{m+1}(\rho)}{J_m(\rho)})^2}{1 + \beta(\frac{J_{m+1}(\rho)}{J_m(\rho)})^2}\right]\tau_{LC} \qquad (15)$$

for each order m. Given the structure of the Bessel functions it is straightforward to verify that the theoretical absolute maximum delay is obtained for the $m = -2$ order and it is equal to $2\tau_{LC}$ [24]. Correspondingly, the theoretical limit for the maximum fractional delay, which is the pulse delay compared to the pulse width, is one. Indeed, in order to avoid distortions, the width of the input pulse has to be within the frequency bandwidth of the two-wave-mixing, which requires a minimum temporal width of the order of $2\tau_{LC}$.

In Fig. 6 is shown the group velocity of the pulse $v_m = d/\Delta t_m$ versus the frequency detuning $\Delta\omega$, for $m = 0$ and $m = -2$. A good agreement between the theoretical prediction and the experimental points is achieved. For $m = 0$ we observe a second branch corresponding to fast-light whereas for $m = -2$ we have only the slow-light branch with a minimum group velocity less than 0.2 mm/s.

The group delay and, therefore, the group velocity can be tuned by changing the experimental parameters, such as the ratio of the pump and signal peak intensity β, the spacing of the refractive index grating Λ, and the nonlinear coefficient n_2. This last one can be changed by varying either the voltage V_0 applied to the LCLV or the pump intensity I_p. As an example, we show in Fig. 7 the behavior of the $m = 0$ order as a function of the pump intensity I_p and of the nonlinear coefficient n_2. The theoretical group delay Δt_0 is plotted together with the experimental points, which are measured for $\Delta\omega = 0$, $\beta = 3$ and $\beta = 30$, a grating spacing $\Lambda = 250$ μm and a pump intensity $I_p = 1.5$ mW/cm². In Fig. 7a we observe that for $\beta = 3$ there is a decrease of Δt_0 for $I_p > 2$ mW/cm². This is due to the dependency of the maximum group delay from the Bessel functions, which, depending on the respective value of I_p and β, can provide a decreasing contribution, as can be seen from Eq. (15). Note that also the argument of the Bessel functions, ρ, depends on β since it is proportional to $\sqrt{I_p I_s}$. On the other side, we see in Fig. 7b that Δt_0 increases monotonically with n_2 for both values of β. Correspondingly, the group velocity can be finely tuned by changing the voltage V_0 applied to the LCLV.
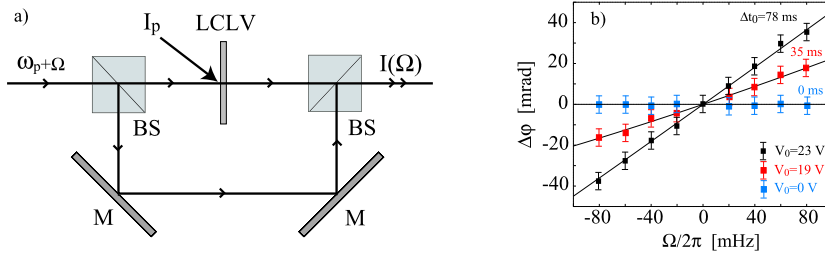
Fig. 8. (Color online.) (a) Schematic diagram of a Mach–Zehnder interferometer with the LCLV operating as a slow-light medium; BS: beam-splitters, M: mirrors. (b) Phase shift detected by the interferometer as a function of the perturbation frequency Ω for different voltages V_0 applied to the LCLV and correspondingly increasing group delays.

5. Mach–Zehnder interferometer with slow-light enhanced sensitivity

The large group delay provided by the two-wave-mixing in the LCLV corresponds to a large group index, a property that can be used to enhance the spectral sensitivity of certain types of interferometers. As an example, we have realized a Mach–Zehnder interferometer in which we have inserted a LCLV [34]. A pump beam is incident on the LCLV and the interferometer is aligned along the direction of the $m = 0$ output order. If we introduce a small frequency perturbation Ω on the input signal, the transmission of the interferometer is given by

$$T = \frac{1}{2}[1 + \cos \Delta\varphi] \qquad (16)$$

where the total phase difference $\Delta\varphi$ is given by the optical path difference ΔL between the two arms of the interferometer and by the slow-light nonlinear phase retardation Φ_0, which, as we have seen before, is a function of the frequency detuning Ω. If the frequency perturbation is small with respect to the bandwidth of the two-wave-mixing, $\Omega < 1/(2\tau_{LC})$, we can write

$$\Phi_0(\Omega) \simeq \Phi_0(0) + \left[\frac{\partial \Phi_0}{\partial \Omega}\right]_0 \Omega = \Phi_0(0) + \Delta t_0 \Omega \qquad (17)$$

Since the group delay is much larger than $\Delta L/c$ (for example, for $\Delta L = 1$ m we have $\Delta L/c \sim 10^{-7}$ s), we can neglect the linear contribution and the total phase shift can be written as

$$\Delta\varphi \simeq \Phi_0(0) + \Delta t_0 \Omega \qquad (18)$$

Therefore, the spectral sensitivity of the interferometer is directly related to the group delay

$$T = \frac{1}{2}\big[1 + \cos\big(\Delta t_0 \Omega + \Phi_0(0)\big)\big] \qquad (19)$$

and the group delay being very large, it is hugely enhanced. Thanks to the tunability of $\Phi_0(0)$ through V_0, in the experiment we have fixed $\Phi_0(0) = \pi/2$, so that $T \propto \sin \Delta t_0 \Omega$ and for small frequency perturbations the detection becomes linear, $T \simeq \Delta t_0 \Omega$, with Δt_0 the large group delay provided by the slow-light process.

In Fig. 8 we report the phase change detected at the output of the interferometer when a small frequency perturbation Ω, created by a piezoelectrically driven mirror, is added on the signal beam. While the interferometer shows no sensitivity when the LCLV is switched off, $V_0 = 0$, we see that the sensitivity largely increases when increasing V_0. The slopes of the detected phase curves are the corresponding group delays provided by the slow-light process in the LCLV.

6. Picometer detection by adaptive holography in the LCLV

As we have seen in Section 3, the slow-light process in the LCLV is induced by a rapid change of the refractive index, which occurs due to the narrow frequency bandwidth of the gain provided by the two-beam coupling. While slow- and fast-light effects exploit the dispersion properties, will see here that the gain counterpart acts as an optical filter and can be used to realize an adaptive holographic interferometer (AHI). The main objective of the adaptive
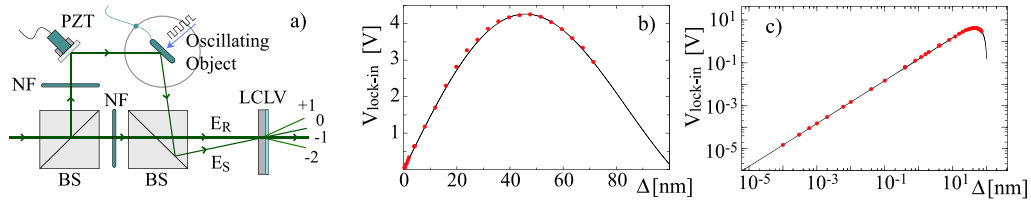
Fig. 9. (Color online.) (a) Schematic diagram of the adaptive holographic system using the LCLV as a narrow frequency bandwidth medium; NF: neutral density filters, PZT: piezoelectrically driven mirror. (b) Signal $V_{\text{lock-in}}$ detected on the $m = -1$ order as a function of the mirror displacement Δ; (c) the same data are plotted in logarithmic scale.

interferometry is to detect frequency phase modulations of optical beams with complex wavefronts, such as speckle beams, characterized by low frequency noise fluctuations, such as given by environmental disturbances when the beam passes, for instance, through the atmosphere, or turbid media or biological tissues. Adaptive holography addresses the problems related to these types of measurements by using an interferometer scheme where the signal beam, carrying the phase modulations, is made to interfere with a reference beam, thus producing an adaptive hologram [35]. This last one is made by a nonlinear medium able to provide a self-reconfigurable index of refraction. An important property of the adaptive hologram is the narrow optical bandwidth, which gives the ability of the system to reject low frequency noise. Because slow- and fast-light effects are related to narrow bandwidth features of the gain, nonlinear wave-mixing processes are naturally good candidates for realizing AHI systems. Another important parameter of AHI is the sensitivity, which is the minimum amplitude of phase modulations detectable when only photon shot noise is present.

Two-wave-mixing in the LCLV provides both a good sensitivity and a narrow frequency bandwidth, and, indeed, can be used to efficiently realize an AHI system [36]. The experimental setup is shown in Fig. 9a. By means of a piezo-electrically driven mirror the signal beam E_s is phase modulated with a sinusoidal oscillation at high frequency Ω and small amplitude Δ. The frequency of the modulation is fixed at $\Omega/2\pi = 1$ kHz, which is much greater than the bandwidth of the two-wave-mixing in the LCLV. The signal beam is sent onto the LCLV together with a reference beam E_R. The optical power of the output beams is measured through a photodiode and a lock-in amplifier synchronized to the frequency Ω of the phase modulation. The amplitude of the phase grating that is generated by the two-wave-mixing inside the LC layer is given by

$$\varphi = 2k\,dn_2 E_R E_s J_0(2k\Delta) \tag{20}$$

Because of the large value of the LCLV nonlinear coefficient n_2, the process is very efficient. The output diffracted beams are easily detected and, in particular, the output optical power at the frequency Ω can be calculated and it is given by

$$\hat{P}_m(\Omega) = 4P_R e^{-\alpha D} K J_m(\varphi) J_{m+1}(\varphi) J_1(2k\Delta) \tag{21}$$

where m is the order of diffraction, $D = 1$ mm the thickness of the photoconductor and $\alpha = 0.3$ cm^{-1} its absorption coefficient. The ratio between the intensity of the reference and signal beam is K and J_m is the Bessel function of first kind and order m.

An important characteristic of the AHI is that when the amplitude of the phase modulation is small the detection is always linear in Δ, at variance with standard interferometers where the detection is linear only for precise values of the optical path difference between the reference and signal beam. The sensitivity of the system is obtained by considering only the photon shot-noise. The signal-to-noise ratio in this case is given by [36]

$$\text{SNR} = \sqrt{\frac{2\eta P_R}{\hbar\omega\Delta f}} e^{\frac{-\alpha D}{2}} \frac{K J_m(\varphi) J_{m+1}(\varphi)}{\sqrt{K^2 J_m^2(\varphi) J_{m+1}^2(\varphi)}} 2k\Delta \tag{22}$$

where $\eta = 0.4$ is the quantum efficiency of the photodiode and $\Delta f = 1$ Hz is the bandwidth of the electronic detection system. The maximum signal to noise ratio is obtained for $m = -1$ and the minimum detectable phase is of the order of 7 nrad/Hz$^{1/2}$. In Fig. 9b, the detected signal $V_{\text{lock-in}}$ is plotted as a function of the mirror displacement Δ, for the $m = -1$ order, for which the theoretical curves predict the maximum sensitivity [36]. The intensity of the optical beam was 3 mW/cm^2 and $K = 5$. In Fig. 9c the same data are plotted in logarithmic scale. We see that the detection is linear for small displacements and that mirror displacements as small as 0.1 pm are detected.
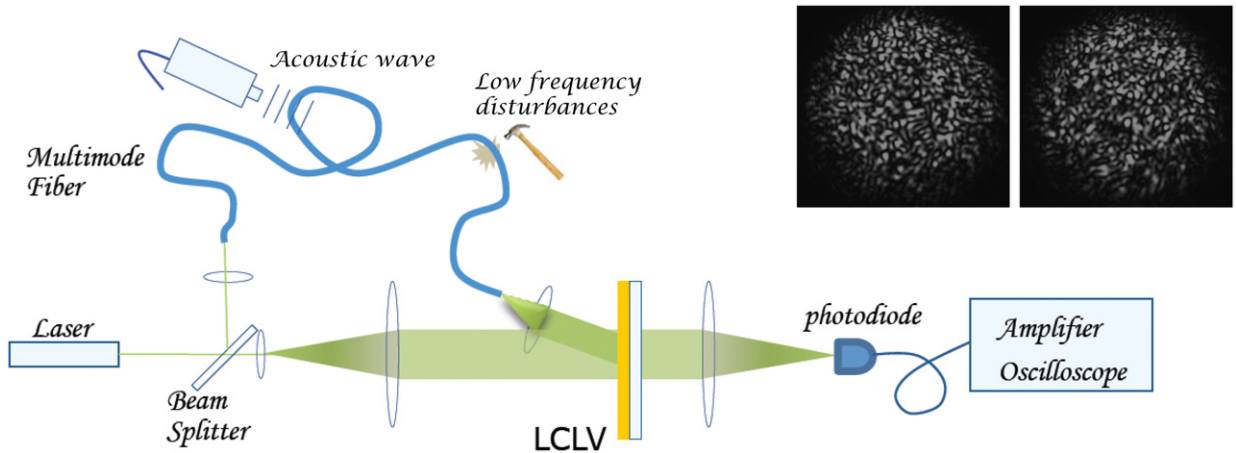
Fig. 10. (Color online.) Schematic setup for the detection of phase modulations of a speckles field. In the insert, the speckles field at the output of the multimode fiber is shown at two different instant times; the time separation between the two images is 0.2 s.
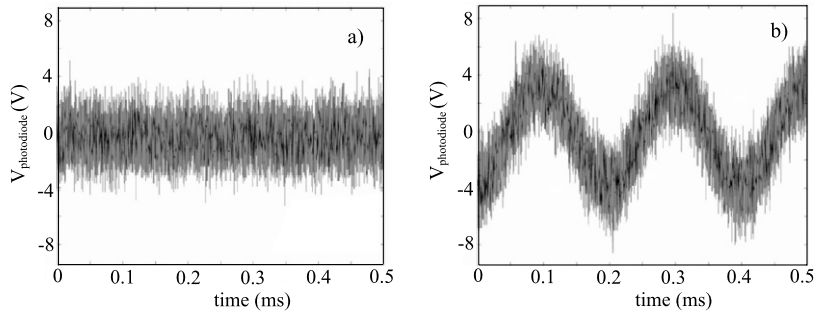

Fig. 11. Signal $V_{photodiode}$ detected as a function of time in the case of (a) a Michelson interferometer and (b) after the LCLV in the AHI system.

Finally, in order to test the ability of the system to work with complex wavefronts, we have performed an experiment in which we take as signal the optical field distribution at the exit of a multimode fiber. The setup is sketched in Fig. 10. A high frequency modulation is created by sending on the fiber an acoustic wave at $\Omega/2\pi = 5$ kHz and low frequency perturbations are induced by local, and small, disturbances, induced, for example, by touching the fiber. At the exit of the fiber, the optical field distribution is a speckles pattern with a slow dynamics, as shown in the inset of Fig. 10. In the case of a classical interferometer the phase modulations of the signal are completely hidden by the noise, as shown in Fig. 11a. In the case of AHI, the two-wave-mixing in the LCLV provides a narrow frequency bandwidth that filters out noise low frequency noise fluctuations, and the acoustic wave modulating the signal can be clearly distinguished. This is evident in Fig. 11b, where it is plotted the time evolution of the photodiode signal measured after the LCLV in the adaptive interferometer setup.

7. Conclusions

In conclusion, liquid crystal light-valves are very attractive media for slow- and fast-light applications since they show a large and tunable group delay and can be employed for interferometric or adaptive holography applications. We have shown that the group velocity in the LCLV can be finely tuned by changing the control parameters of the two-wave-mixing, in particular by varying the strength of the nonlinearity, which is realized experimentally by changing the amplitude of the applied voltage or the intensity of the pump beam. The theoretical description is very general and can be applied to other thin nonlinear media, provided they allow performing beam coupling experiments.

References

[1] R.W. Boyd, D.J. Gauthier, in: E. Wolf (Ed.), Progress in Optics, vol. 43, Elsevier Science, Amsterdam, 2002, pp. 497–530.
[2] F. Xia, L. Sekaric, Y. Vlasov, Nature Photonics 1 (2007) 65.
[3] Z. Shi, R.W. Boyd, D.J. Gauthier, C.C. Dudley, Opt. Lett. 32 (2007) 915.
[4] Z. Shi, R.W. Boyd, Phys. Rev. Lett. 99 (2007) 240801.
[5] G.S. Pati, M. Salit, K. Salit, M.S. Shahriar, Phys. Rev. Lett. 99 (2007) 133601.
[6] H.N. Yum, M. Salit, G.S. Pati, S. Tseng, P.R. Hemmer, M.S. Shahriar, Opt. Express 16 (2008) 20448.
[7] S.E. Harris, Phys. Today 50 (1997) 36.
[8] A. Kasapi, M. Jain, G.Y. Yin, S.E. Harris, Phys. Rev. Lett. 74 (1995) 2447.
[9] L.V. Hau, S.E. Harris, Z. Dutton, C.H. Behroozi, Nature (London) 397 (1999) 594.
[10] M.S. Bigelow, N.N. Lepeshkin, R.W. Boyd, Phys. Rev. Lett. 90 (2003) 113903.
[11] Y.A. Vlasov, M. O'Boyle, H.F. Hamann, S.J. McNab, Nature 428 (2005) 65.
[12] T. Baba, Nature Photonics 2 (2008) 465.
[13] J. Mork, F. Öhman, M. van der Poel, Y. Chen, P. Lunnemann, K. Yvind, Laser & Photon. Rev. (2008) 1–15.
[14] S. Tonda-Goldstein, P. Berger, D. Dolfi, J. Chazelas, J.P. Huignard, Proceedings of the European Microwave Association, 2008.
[15] N.V. Kukhtarev, V.B. Markov, S.G. Odulov, M.S. Soskin, V.L. Vinetskii, Ferroelectrics 22 (1979) 949.
[16] J.P. Huignard, A. Marrakchi, Opt. Lett. 6 (1981) 622.
[17] A. Marrakchi, J.P. Huignard, P. Gunter, Appl. Phys. Lett. 24 (1981) 131.
[18] A. Yariv, D.M. Pepper, Opt. Lett. 1 (1977) 16.
[19] E. Podivilov, B. Sturman, A. Shumelyuk, S. Odoulov, Phys. Rev. Lett. 91 (2003) 083902.
[20] A. Shumelyuk, K. Shcherbin, S. Odoulov, B. Sturman, E. Podivilov, K. Buse, Phys. Rev. Lett. 93 (2004) 243604.
[21] G. Zhang, R. Dong, F. Bo, J. Xu, Appl. Opt. 43 (2004) 1167;
     G. Zhang, F. Bo, R. Dong, J. Xu, Phys. Rev. Lett. 93 (2004) 133903.
[22] Y. Okawachi, M.S. Bigelow, J.E. Sharping, Z. Zhu, A. Schweinsberg, D.J. Gauthier, R.W. Boyd, A.L. Gaeta, Phys. Rev. Lett. 94 (2005) 153902.
[23] L. Thévenaz, Nature Photonics 2 (2008) 474.
[24] S. Residori, U. Bortolozzo, J.P. Huignard, Phys. Rev. Lett. 100 (2008) 203603.
[25] R.M. Camacho, C.J. Broadbent, I. Ali-Khan, J.C. Howell, Phys. Rev. Lett. 98 (2007) 043902.
[26] P.K. Vudyasetu, R.M. Camacho, J.C. Howell, Phys. Rev. Lett. 100 (2008) 123903.
[27] P. Aubourg, J.P. Huignard, M. Hareng, R.A. Mullen, Appl. Opt. 21 (1982) 3706.
[28] A. Brignon, I. Bongrand, B. Loiseaux, J.P. Huignard, Opt. Lett. 22 (4) (1997) 1855.
[29] P. Gunter, J.P. Huignard, Photorefractive Materials and Their Applications 1, Springer Science, New York, 2006.
[30] P.G. De Gennes, J. Prost, The Physics of Liquid Crystals, second ed., Oxford Science Publications, Clarendon Press, 1993.
[31] A. Yariv, Optical Waves in Crystals, John Wiley & Sons, New Jersey, 2003, pp. 354–358.
[32] U. Bortolozzo, S. Residori, J.P. Huignard, Opt. Lett. 31 (2006) 2166.
[33] U. Bortolozzo, S. Residori, J.P. Huignard, Phys. Rev. A 79 (2009) 053835.
[34] S. Residori, U. Bortolozzo, J.P. Huignard, Appl. Phys. B 95 (2009) 551.
[35] A.A. Kamshilin, R.V. Romashko, Y.N. Kulchin, J. Appl. Phys. 105 (2009) 031101-11.
[36] U. Bortolozzo, S. Residori, J.P. Huignard, Opt. Lett. 34 (2009) 2006–2008.